

AperTO - Archivio Istituzionale Open Access dell'Università di Torino

## Characterization and Modeling of Reversible CO<sub>2</sub> Capture from Wet Streams by a MgO/Zelite Y Nanocomposite

### This is the author's manuscript

*Original Citation:*

*Availability:*

This version is available <http://hdl.handle.net/2318/1707409> since 2020-02-28T14:20:32Z

*Published version:*

DOI:10.1021/acs.jpcc.9b01399

*Terms of use:*

Open Access

Anyone can freely access the full text of works made available as "Open Access". Works made available under a Creative Commons license can be used according to the terms and conditions of said license. Use of all other works requires consent of the right holder (author or publisher) if not exempted from copyright protection by the applicable law.

(Article begins on next page)

# Characterization and modelling of reversible CO<sub>2</sub> capture from wet streams by a MgO/zeolite Y nanocomposite

*Matteo Signorile<sup>1</sup> †, Jenny G. Vitillo<sup>2</sup> †\*, Maddalena D'Amore<sup>1</sup>, Valentina Crocellà<sup>1</sup>, Gabriele Ricchiardi<sup>1\*</sup> and Silvia Bordiga<sup>1</sup>*

<sup>1</sup>Università di Torino, Dipartimento di Chimica and NIS Interdepartment Centre, Via Giuria 7, 10125 Torino, Italy.

<sup>2</sup> Department of Science and High Technology and INSTM, Università degli Studi dell'Insubria, Via Valleggio 9, I-22100 Como, Italy.

†These authors have equally contributed to this work.

KEYWORDS: CO<sub>2</sub> adsorption, carbon capture, basic zeolites, magnesium oxide, DFT, IR spectroscopy.

The synthesis of CO<sub>2</sub> sorbents capable of working on combustion flue gases is a challenging topic in the field of carbon capture and sequestration. Indeed, the presence of moisture in combustion exhausts makes most of the materials capturing CO<sub>2</sub> through physisorption ineffective, being their

larger affinity for H<sub>2</sub>O than for CO<sub>2</sub>. In this work, we investigate a novel nanocomposite sorbent based on a Mg overexchanged zeolite Y (MgOHY), showing single Mg<sup>2+</sup> ions and nanoconfined (MgO)<sub>n</sub> clusters. The interaction of CO<sub>2</sub> with the material is studied thoroughly by combining IR spectroscopy and simulation, comparing dry and wet conditions. IR spectroscopy shows that, while in dry conditions the adsorption is mainly driven by the Mg<sup>2+</sup> ions, in wet ones the (MgO)<sub>n</sub> clusters react with carbon dioxide by forming (bi)carbonate-like species. These easily decompose at mild temperatures (25-200 °C). DFT simulations are used to investigate the origin of the CO<sub>2</sub> interaction with representative (MgO)<sub>n</sub> clusters in the periodic zeolite structure and their enthalpy of formation as function of the water coverage. The calculations disclose a synergic effect between CO<sub>2</sub> and H<sub>2</sub>O that, while favoring the CO<sub>2</sub> fixation, brings to the formation of (bi)carbonate-like species less stable than those formed in absence of water.

## Introduction

Massive post-combustion CO<sub>2</sub> capture requires efficient, robust and economically viable processes.<sup>1</sup> Scrubbers based on aqueous amine solutions are considered the most mature technologies among those proposed, being a number of industrial implementations already available, in the context of natural gas sweetening.<sup>2</sup> Energetic and environmental limitations of these processes boost the search for alternative ones and related materials. One notable direction of research is the development of solid adsorbents, because they intrinsically overcome the main limitation of aqueous solutions (e.g. the high energy consumption related to the use of water as solvent).<sup>3</sup> The ideal solid CO<sub>2</sub> capture material should: (i) possess high CO<sub>2</sub> uptake and affinity towards CO<sub>2</sub>; (ii) release CO<sub>2</sub> by means of a moderate temperature or pressure swing; (iii) possess a low heat capacity to minimize the energy consumption; (iv) preserve its structure and reactivity

upon several thousand adsorption/desorption cycles and (v) be compatible with post combustion wet streams.<sup>4</sup> This last point poses severe challenges. Several classes of materials have been proposed, including metal organic frameworks (MOFs), basic oxides and ion-exchanged zeolites. Widely available inorganic materials like oxides and zeolites are promising in terms of cost and robustness. Moreover, basic oxides have very high theoretical CO<sub>2</sub> capacities, by fixing CO<sub>2</sub> through their conversion to carbonates and bicarbonates<sup>5</sup>. However, these products are very stable and their decomposition temperature is too high for practical reversible applications at low (RT-200 °C) and intermediate temperatures (200-400 °C).<sup>6,7</sup> MgO has the lowest regeneration temperature among oxides, though falling around 500°C.<sup>8</sup> Moreover, the charging and the discharging processes are characterized by very slow kinetics, limiting *de facto* the CO<sub>2</sub> uptake to a few percent of the full stoichiometric capacity.<sup>8</sup> Alkaline and alkaline-earth zeolites are effective and reversible weakly basic solids for CO<sub>2</sub> capture from dry streams.<sup>9,10</sup> As a matter of fact, zeolite 13X (FAU framework) is considered the reference material in both adsorption and separation studies.<sup>11</sup> Nevertheless, the high hydrophilicity of zeolites with low Si/Al ratio (required to increase the number of available cations) hinders their use in wet CO<sub>2</sub> streams, being these materials fast poisoned by water.<sup>12-14</sup>

Nanostructured porous materials with active guest species able to chemically fix CO<sub>2</sub> have been proposed to overcome these limitations, based on zeolites and MOFs as the microporous scaffolds.<sup>8,15</sup> We have developed an MgO/zeolite Y nanocomposite (named hereafter MgOHY), showing in our preliminary investigation to be a promising candidate for CO<sub>2</sub> capture. The material under study is an over-exchanged zeolite Y obtained by impregnation of the acidic form of the zeolite (HY) with a Mg(NO<sub>3</sub>)<sub>2</sub>·6H<sub>2</sub>O solution, followed by a carefully controlled thermal treatment optimized for preserving the zeolite structure and maximize MgO dispersion. The synthesis and

characterization of the material are described in a previous paper,<sup>16</sup> along with main differences among the present MgO/zeolite system and those already reported in the literature. In this work, we describe the fundamental CO<sub>2</sub> and water adsorption properties of the material and we interpret them in terms of molecular interactions by means of spectroscopic experiments and quantum mechanical modelling. IR spectroscopy has been applied in order to disclose the nature of the CO<sub>2</sub>-based species formed over the MgOHY sample, both in dry and wet conditions. The material was also tested as CO<sub>2</sub> scrubber in a set-up simulating a post combustion capture process, where IR spectroscopy was the tool used to monitor both the adsorption and the desorption process. Kohn Sham density functional methods (KS-DFT) have been employed to obtain an atomistic description of the species involved in the process and their relative stability. The complexity of the MgOHY system, which cannot be fully explored by computational methods, was handled by means of five periodic models considering representative (MgO)<sub>n</sub> units in the zeolite pores, designed and fully described in Ref. <sup>16</sup>. Both CO<sub>2</sub> molecular adducts and (bi)carbonate-like species were considered in the simulation. The formation enthalpy of the carbonate species was investigated for selected models at increasing hydration degree (H<sub>2</sub>O to CO<sub>2</sub> ratio from 0 to 3).

## **Materials and Methods**

*Materials.* The synthesis of the MgOHY material is described in ref. <sup>16</sup>. MgOHY and HY samples were stored in a glove box and their contact with air was minimized to avoid carbonation. Two different MgO samples were used as reference materials. For the sake of comparison of the volumetric measurements, an MgO sample was prepared from a magnesium nitrate solution with the same procedure adopted for the MgOHY material.<sup>16</sup> The low surface area of this MgO sample makes it not suitable for IR spectroscopy measurements. As a reference for spectroscopic studies,

a high surface area MgO obtained by chemical vapor deposition (CVD) was adopted, whose synthesis and characterization are described in ref. <sup>17</sup>

*Volumetry.* Excess carbon dioxide adsorption isotherms were measured on a commercial volumetric apparatus (Micromeritics ASAP 2020, Norcross GA) at 25 °C. Prior to the measurements, the HY and MgOHY powders were degassed at 400°C on a vacuum line equipped with a turbomolecular pump and then the samples were transferred in the measurement cell in a glove box. The sample temperature was maintained constant by using an external isothermal liquid bath (Julabo F25-EH). All the reported quantities are affected by an error of 10%.

*In situ IR spectra in static conditions* were collected for the sake of fundamental understanding of the adsorption processes of CO<sub>2</sub> and/or H<sub>2</sub>O. Spectra collection has been performed with a Bruker Vertex 70 spectrophotometer equipped with a Mercury Cadmium Telluride (MCT) cryodetector, at 2 cm<sup>-1</sup> resolution and averaging 32 scans, at the temperature reached by samples under the IR beam (BT, ~50 °C). The samples were examined in the form of self-supporting pellets, mechanically protected by a pure gold frame. Before each measurement, all samples were thermally activated in vacuo at 400 °C (for HY and MgOHY) or 700 °C (for pure MgO) by using a home-made quartz IR cell, equipped with KBr windows and characterized by a very small optical path (2 mm). The cell was connected to a glass vacuum line, equipped with a turbo molecular pump (capable of a residual pressure < 10<sup>-4</sup> mbar), that allows collecting measurements under controlled atmosphere. After thermal activation, the materials were contacted with the different molecular probes: (i) H<sub>2</sub>O; (ii) CO<sub>2</sub> (“dry CO<sub>2</sub>“ in the following); or (ii) CO<sub>2</sub>/H<sub>2</sub>O mixture (“wet CO<sub>2</sub>“). Concerning the spectra obtained for the CO<sub>2</sub>/H<sub>2</sub>O mixture, materials were first contacted with CO<sub>2</sub>, then H<sub>2</sub>O vapors ( $p \sim 20$  mbar) were admitted in the measurement cell. The hydration process has been monitored in time for the MgOHY sample.

*In situ IR-MS spectroscopy using reagent gas flow* has been performed in order to monitor the CO<sub>2</sub>/H<sub>2</sub>O co-adsorption and desorption processes under conditions relevant for potential applications. As in static IR experiments, gold enveloped pelletized samples (10 mg, pressed at 10 MPa) were placed inside a commercial IR reactor cell (AABSPEC, #2000-A multimode), which allows infrared spectra to be recorded in the RT-950 °C temperature range. Spectra were collected by a Perkin Elmer System 2000 IR spectrophotometer, equipped with a MCT detector, at a resolution of 2 cm<sup>-1</sup> and averaging 64 scans. Accurate control of the flow rate into the reactor cell of each gas component was accomplished through individual mass flow controllers, using helium as the inert balance. All the lines upstream and downstream the reactor have been heated at 150°C to prevent H<sub>2</sub>O condensation. The outlet gas composition has been online monitored by a mass spectrometer (MS, Thermo Electron Smart IQ+ Residual Gas Analyzer, equipped with a triple filter quadrupole and a dual detector), simultaneously collecting the 4 (He), 16 (O<sub>2</sub>, CO<sub>2</sub>), 18 (H<sub>2</sub>O), 28 (CO<sub>2</sub>) 32 (O<sub>2</sub>) and 44 amu (CO<sub>2</sub>) signals. Before each measurement, the samples were activated at 400°C (1 °C/min up to 250°C, 5 °C/min up to 400°C, isotherm at 400 °C for 30 min) in a 15 ml/min He gas flow and the dehydration degree was checked in real time through IR spectroscopy. The system was then allowed to cool at RT, before exposure to a 15.4 ml/min flow with volume composition: 90.2%He/6.5%CO<sub>2</sub>/2.6%H<sub>2</sub>O/0.6%Ar. The composition was obtained by mixing two separated flows: (i) 5 ml/min He flow, passing through a saturator where the water was kept at 40.8°C (corresponding to 2.6 vol% H<sub>2</sub>O); (ii) 10 ml/min 10% CO<sub>2</sub>/1% Ar/ 89% He. The overall process was monitored overnight at RT by the FTIR-MS apparatus. The desorption experiment has been carried out by switching back to the dry helium flow (15 ml/min) and monitoring the system for 1 h at RT, before heating it up to 500°C with a rate of 3 °C/min. IR spectra have been collected throughout every 10°C, while monitoring the downstream by MS.

*Periodic DFT calculations.* The details of the MgOHY model building are given in a previous publication.<sup>16</sup> It suffices to recall here that the acidic zeolite was modelled as a (H<sub>13</sub>O<sub>96</sub>Al<sub>13</sub>Si<sub>35</sub>, Si/Al= 2.692) periodic model with P1 symmetry, with random Al distribution compliant with the Löwenstein rule. Four MgO formula units per unit cell were added in the HY model, simulating a variety of ion exchange and cluster structures. In this paper, we discuss the interaction of CO<sub>2</sub> and H<sub>2</sub>O (individually or combined) with five low energy MgOHY structures obtained in our previous investigation.

All calculations were performed with the CRYSTAL17 package, a periodic *quantum mechanical* code based on atom-centered Gaussian basis sets<sup>18</sup>. Notably, the use of atom-centered basis sets in this code allows the accurate and easy evaluation of the exact Hartree Fock exchange, so that it can efficiently deal with hybrid functionals for periodic systems. Geometry optimizations were performed using the hybrid B3LYP functional.<sup>19,20</sup> Dispersion interactions, whose importance in effectively modeling adsorption processes in porous solids has been demonstrated,<sup>21–24</sup> were accounted through an empirical correction, where the total computed energy is given by Equation

1

$$E_{\text{DFT-D}} = E_{\text{DFT}} + E_{\text{disp}} \quad (1)$$

where  $E_{\text{disp}}$  is the empirical D2 dispersion correction scheme proposed by Grimme for molecules (see Equation 2)<sup>25</sup> and re-parametrized for crystalline systems (referred as B3LYP-D\*):<sup>26</sup>

$$E_{\text{disp}} = S_6 \sum_g \sum_{ij} f(R_{ij,g}) \frac{C_6^{ij}}{R_{ij,g}^6} \quad (2)$$

A double- $\zeta$  plus polarization quality basis set was adopted for the zeolite atoms (Si, Al, O).<sup>27,28</sup>

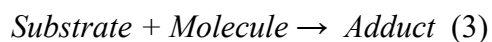
The more extended VTZ2P basis sets of Ahlrichs et al.<sup>29</sup> have been adopted on C and O (for both



CO<sub>2</sub> and MgO) atoms, and that of Ugliengo et al.<sup>30</sup> on Mg. Basis Set Superposition Error (BSSE) has been evaluated for the H<sub>2</sub>O and CO<sub>2</sub> adducts, obtaining values in the 4-15 kJ/mol range. Given these low values, no correction was applied to the binding energies, in order to preserve consistency between the results for molecular adsorption and carbonate formation (where BSSE is not clearly defined).

Concerning computational parameters, the five threshold parameters  $T_i$  determining the level of accuracy of mono- and bi-electronic integrals were set to  $10^{-8}$  for ( $T_1$ - $T_4$ ) and  $10^{-18}$  for  $T_5$  {TOLINTEG 7 7 7 7 18}. The threshold on the SCF energy was set to  $10^{-8}$  Ha for the geometry optimizations and to  $10^{-10}$  Ha for the Hessian calculations. The DFT exchange-correlation contribution and its gradient were evaluated by numerical integration over the unit cell volume according to the method derived by Becke for molecules<sup>19</sup> on a pruned grid with 75 radial and 974 angular points. The reciprocal space was sampled at the  $\Gamma$  point. Geometry relaxations were performed by allowing both atomic positions and cell parameters to be optimized simultaneously. Enthalpies and Gibbs free energies were estimated at standard conditions through a reduced Hessian approach, including in the calculation only the atoms belonging to CO<sub>2</sub>, H<sub>2</sub>O, MgO clusters and the O atoms bonding them to the zeolitic framework (i.e. the most significant ones for the adsorption processes). All the parameters not explicitly mentioned above have been set to their default values (see the CRYSTAL17 user's manual for further details).<sup>31</sup>

Adsorption of CO<sub>2</sub> and/or H<sub>2</sub>O over MgOHY models (eventually already interacting with pre-adsorbed molecules) has been simulated considering the following process (Equation 3):



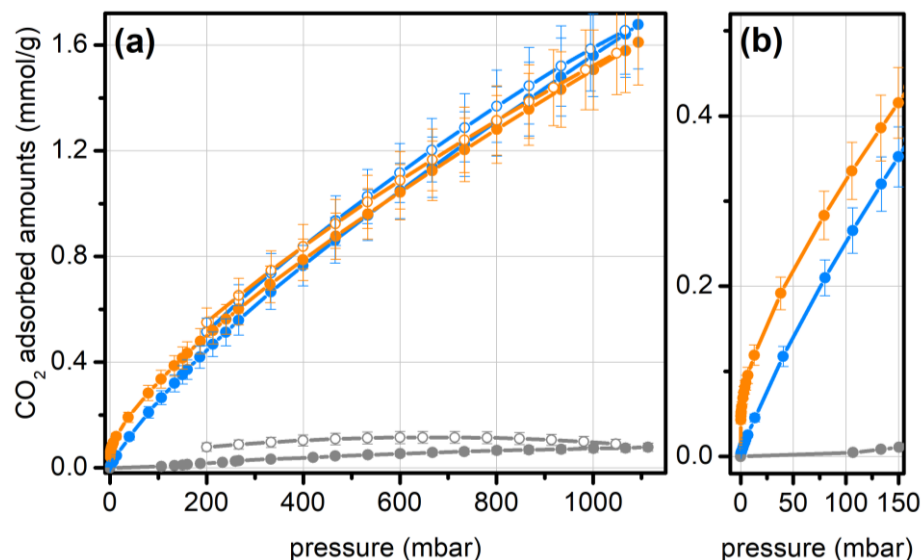
and the corresponding adsorption/reaction electronic energies ( $\Delta E$ ), enthalpies ( $\Delta H$ ) and Gibbs free energies ( $\Delta G$ ) have been computed accordingly as reported in Equation 4:

$$\Delta X = X_{\text{Adduct}} - X_{\text{Substrate}} - X_{\text{Molecule}} \quad (X = E, H \text{ or } G) \quad (4)$$

## Results and Discussion

*Volumetric measurements of dry CO<sub>2</sub> adsorption.* As a preliminary characterization of the material, CO<sub>2</sub> sorption isotherms were measured at 25°C for MgOHY, for its parent HY zeolite and for a bulk MgO sample synthesized using the same protocol used for MgOHY (Figure 1). The incorporation of Mg-based species in the zeolite pores causes a 10% decrease of the surface area of the material, as previously reported.<sup>16</sup> In spite of the lower surface area, MgOHY (orange line) shows a higher CO<sub>2</sub> uptake than HY (blue line) at  $p < 400$  mbar, while the two materials tend to behave similarly at higher pressures as adsorption is here dominated by the available pore volume. The uptake capacity associated with the introduction of the Mg-based species is significant at  $p < 150$  mbar, which is the range of partial pressure of interest in post-combustion capture. The bulk MgO reference material (grey line) shows a not negligible CO<sub>2</sub> adsorption capacity in spite of its three order of magnitude lower surface area ( $< 10 \text{ m}^2 \text{ g}^{-1}$ ). Nevertheless, MgO, unlike the zeolitic materials, shows a large hysteresis between the adsorption (filled scatters) and the desorption run (empty scatters) due to the irreversibility of the absorption process at RT. Interestingly, the MgOHY isotherm shows a good reversibility of the CO<sub>2</sub> adsorption process.

The CO<sub>2</sub> interaction with the three materials and the reversibility of its adsorption have been thus thoroughly studied with infrared spectroscopic methods as described hereafter in order to get information on the species involved in the adsorption process.

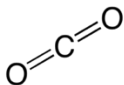
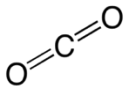
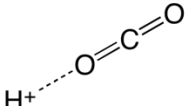
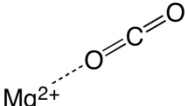
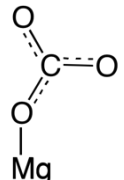
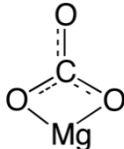
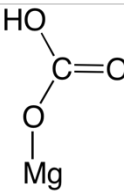


**Figure 1.** Excess CO<sub>2</sub> sorption isotherms recorded at room temperature on MgOHY (orange lines) and HY (light blue lines) activated in vacuum at 400 °C. Grey lines report the data obtained on an MgO material synthesized from magnesium nitrate hexahydrated using the same protocol adopted for MgOHY. (a) pressure range: 0-1.1 bar. (b) pressure range: 0-0.15 bar. Adsorption branch: full scatters. Desorption branch: empty scatters.

*In situ IR spectroscopy* allowed detecting the species formed upon the interaction between the MgOHY zeolite and CO<sub>2</sub> in both dry and wet conditions, in order to verify the formation of different species and their relative stability with respect to the pure phases, HY and MgO. An overview of the main possible CO<sub>2</sub> species expected upon interaction with our samples is given in Table 1 along with their IR fingerprints. Several surface structures are expected, giving rise to significant shifts to the vibrational modes of CO<sub>2</sub> or even completely altering them if reactions take place. We remind here that CO<sub>2</sub> asymmetric stretching frequency ( $\nu_3$ ) shifts of about -11 cm<sup>-1</sup> with respect to its gas phase value when adsorbed in an apolar microporous material by matrix

effect (see Table 1 and refs. 31 and 32 for details). This value should be used in order to correctly evaluate the  $\nu_3$  shift in these materials.

**Table 1.** Vibrational stretching frequencies of CO<sub>2</sub> in relevant states or interacting with specific sites of reference materials.

Species		Adsorbent	Frequency (cm <sup>-1</sup> )	Mode	Refs.
Gas phase		-	2349	$\nu_3(\text{CO}_2)$	32
Gas phase in a microporous matrix		Silicalite	2338	$\nu_3(\text{CO}_2)$	32,33
Brønsted site-CO <sub>2</sub> adduct		HY	2342, 2353	$\nu_3(\text{CO}_2)$	34
Linear Mg <sup>2+</sup> -CO <sub>2</sub> adduct		MgO	2342, 2358, 2382 <sup>a</sup>	$\nu_3(\text{CO}_2)$	35
		Na,Mg-ETS-10	2365	$\nu_3(\text{CO}_2)$	36
		Mg-MOF-74	2353	$\nu_3(\text{CO}_2)$	37
Monodentate Mg carbonate-like		MgO	1520-1550	$\nu_{\text{asym}}(\text{CO}_3)$	38
			1390-1410	$\nu_{\text{sym}}(\text{CO}_3)$	
Bidentate Mg carbonate-like		MgO	1630-1670	$\nu_{\text{asym}}(\text{CO}_3)$	38
			1275-1325	$\nu_{\text{sym}}(\text{CO}_3)$	
Mg bicarbonate-like		MgO	1655	$\nu_{\text{asym}}(\text{C=O})$	38
			1405	$\nu_{\text{sym}}(\text{C=O})$	

In the case CO<sub>2</sub> is linearly physisorbed over acid sites (*i.e.* Brønsted acid protons and/or Lewis acidic Mg<sup>2+</sup> sites, spectral range 2500-2338 cm<sup>-1</sup>), a blue-shift of  $\nu_3$  is observed, whose extent is correlated with the acid strength of the site (the stronger the site, the higher the shift). In the event CO<sub>2</sub> reacts with basic sites (e.g. O atoms bridging Mg<sup>2+</sup> sites in nanoclusters, as well as their Mg-OH terminations), (bi)carbonate-like species are generated, whose specific symmetric ( $\nu_{\text{sym}}$ ) and asymmetric ( $\nu_{\text{asym}}$ ) vibrational fingerprints are observed in the 1700-1250 cm<sup>-1</sup> region. On heterogeneous systems, these vibrational modes are affected by the local environment surrounding the (bi)carbonate-like species, thus a range of frequencies (rather than a well-defined value) is representative for a given family of structures. Still, they can be distinguished and classified on the basis of their direct relation with the closest Mg<sup>2+</sup> sites, *e.g.* giving rise to monodentate carbonates, bidentate carbonates, *etc.*<sup>38</sup>

HY and MgOHY were activated in vacuo at 400 °C to remove any possibly adsorbed species, and in particular water. The IR spectra of the pristine and activated samples are reported in Figure S1 of the Supporting Information, together with a detailed discussion of their assignment (see also ref. 16). These results show that: a) the HY and MgOHY samples are strongly hydrophilic, with MgOHY having a higher hydrophilicity; b) the introduction of MgO in the zeolite does not cause the complete consumption of the acidic protons; c) the presence of Mg-OH groups is observed also in the dehydrated sample, and d) some bands possibly due to residual nitrates or carbonates are detected. Figure 2 reports the IR spectra of HY, MgOHY and MgO upon interaction with pure CO<sub>2</sub> (“dry CO<sub>2</sub>”, part a) and CO<sub>2</sub>+H<sub>2</sub>O (“wet CO<sub>2</sub>”, part b). The plots show the spectral regions relative to linear CO<sub>2</sub> complexes (2500-2200 cm<sup>-1</sup>) and to (bi)carbonate-like species (1800-1200 cm<sup>-1</sup>). A detail of the linear adducts region upon CO<sub>2</sub> adsorption is reported in Figure S2, for both dry and wet conditions.

Concerning dry CO<sub>2</sub> adsorption, the only clear spectroscopic evidence of the presence of CO<sub>2</sub> on the HY sample (light blue line) is a band at 2350 cm<sup>-1</sup>, associated to the  $\nu_3$  vibrational mode of CO<sub>2</sub> perturbed by Brønsted acid sites (see Table 1).<sup>34</sup> Conversely, the spectrum appears identical to that recorded after activation in the range of carbonate-like species. When dry CO<sub>2</sub> is dosed on pure MgO (grey line) we observe, in the high frequencies range, the spectroscopic fingerprints of linear Mg<sup>2+</sup>-CO<sub>2</sub> adducts on MgO flat surfaces, characterized by a main band at 2354 cm<sup>-1</sup>, two minor contributions at 2344 and 2362 cm<sup>-1</sup> (due to the partially hindered rotovibrational components) and a weak band at 2380 cm<sup>-1</sup> (ascribable to linear CO<sub>2</sub> adsorbed on 4- and 3-coordinated Mg<sup>2+</sup> sites).<sup>35</sup> In the carbonates region, the MgO sample contacted with dry CO<sub>2</sub> shows three main band envelopes at (i) 1725-1575 cm<sup>-1</sup>, (ii) 1575-1450 cm<sup>-1</sup> and (iii) 1450-1300 cm<sup>-1</sup> that can be associated to mono- and bidentate carbonates and to bicarbonate species respectively.<sup>38</sup> These species are irreversible upon prolonged pumping at RT and then they are those at the origin of the hysteresis observed in the volumetric measurements (grey line, Figure 1). Dry CO<sub>2</sub> dosed on MgOHY (orange line) gives rise to complex intense bands in the region of linearly coordinated CO<sub>2</sub>. In particular, we observe a main component with a maximum at 2370 cm<sup>-1</sup> and extending toward higher frequencies, ascribable to CO<sub>2</sub> linearly coordinated to Mg<sup>2+</sup> cations (see Table 1). The component at 2350 cm<sup>-1</sup> (shoulder) can be assigned to CO<sub>2</sub> linearly coordinated to the residual fraction of Brønsted acidic sites. Conversely, no major changes are observed in the carbonate region, apart a weak band at 1539 cm<sup>-1</sup>, falling in the range of frequencies proper of mono-dentate carbonates.<sup>38</sup> These results suggest that, in dry conditions, the MgOHY material binds CO<sub>2</sub> preferentially as a molecular complex with limited formation of carbonate-like species. The larger CO<sub>2</sub> uptake observed in Figure 1 for MgOHY with respect to HY for pressures lower than 150 mbar is then associated to the larger polarity of the Mg<sup>2+</sup> ions with respect to the protons.

Part (b) of Figure 2 illustrates the effect of dosing wet CO<sub>2</sub> (see the experimental section for details). For both HY (blue curve) and MgOHY (red curve), the presence of water causes a decrease of the intensity of the signals associated to  $\nu_3$  and its shift to 2343 cm<sup>-1</sup>, indicating the coordination of CO<sub>2</sub> to less positively charged centers than in the dry case. They are likely water molecules directly coordinated to the zeolite counterions, being able to displace CO<sub>2</sub> from the Mg<sup>2+</sup>/H<sup>+</sup> sites because of their higher adsorption energy. In the 1800-1200 cm<sup>-1</sup> region, the two zeolite samples behave differently. The HY sample does not show the formation of any carbonates and only the strong band due to the  $\delta(\text{HOH})$  bending mode of water is evident (~1630 cm<sup>-1</sup>). For MgOHY, several bands appear, associated to (bi)carbonates-like species. This different behavior indicates that while in HY water only decreases the intensity of the signals associated to molecular adsorbed CO<sub>2</sub>, in MgOHY this decrease is compensated by the formation of chemisorbed species. The asymmetric shape of the signal associated to the  $\delta(\text{HOH})$  mode of water in MgOHY (here tailed toward higher wavenumbers), suggests the presence of some bidentate carbonates (maximum expected at 1670 cm<sup>-1</sup>), also confirmed by the growth of the symmetric component at 1310 cm<sup>-1</sup>.<sup>38</sup> Furthermore, the formation of bicarbonates (characterized by bands at 1655 cm<sup>-1</sup> and 1405 cm<sup>-1</sup>) cannot be excluded. The growth of additional absorption at lower frequencies (component at 1530 cm<sup>-1</sup> and a broad absorption extending below 1400 cm<sup>-1</sup>) suggests the formation of some monodentate carbonates too. However, as their fingerprints are mixed with bands already present on the MgOHY background (see Figure S1 and its discussion), the true intensity of these signals (i.e. their abundance) cannot be properly assessed. Moreover, the increased intensity of the baseline in this region suggests that these species are formed, but with heterogeneous local coordination structures as reflected by the very broad IR bands. In the case of the MgO sample (grey line), while the signals associated to CO<sub>2</sub>-Mg<sup>2+</sup> have an almost null

intensity, the carbonate bands reach intensities saturating the MCT detector, thus preventing further considerations on their speciation and relative abundance. The increase in the reaction kinetics in presence of water for both MgOHY and MgO is in agreement with previous reports, showing that CO<sub>2</sub> fixation on MgO is faster in presence of hydroxyl species.<sup>8</sup> It is noteworthy that the (bi)carbonate-like species formed on MgOHY are fully reversible *in vacuo* at the remarkably low temperature of 250 °C (red and grey lines in Figure 2c, respectively), whereas they persist in the case of pure MgO. These species are slightly less stable than those reported for MgO supported on SBA-15<sup>39</sup> and on KNaX with similar Mg loading.<sup>40</sup>

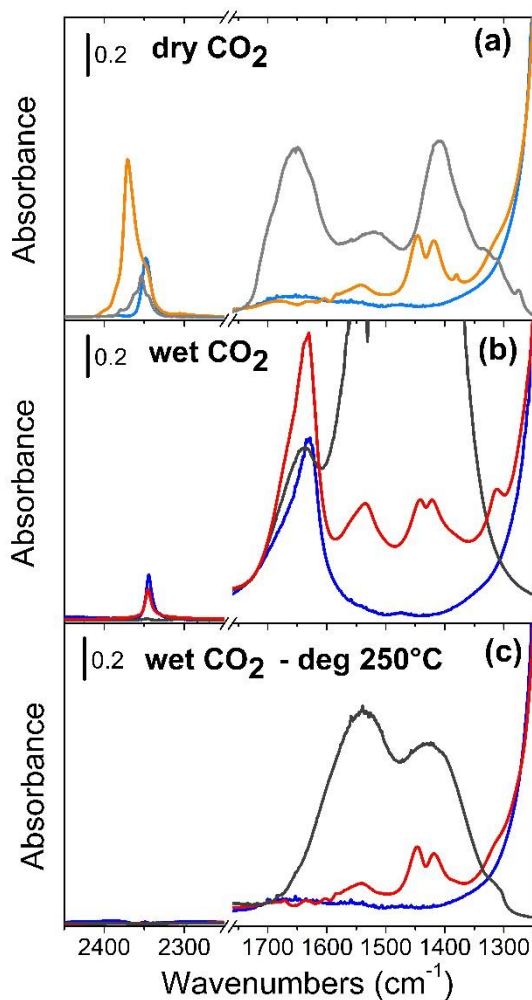




**Figure 2.** IR spectra in the spectral regions relative to  $\text{Mg}^{2+}$ - $\text{CO}_2$  linear complexes ( $2500\text{-}2200\text{ cm}^{-1}$ ) and to (bi)carbonate-like species ( $1800\text{-}1200\text{ cm}^{-1}$ ) of: (a) samples after contact with 5 mbar of  $\text{CO}_2$  at BT: HY (light blue curve), MgO (light grey curve), and MgOHY (orange curve); (b) samples contacted with a mixture of  $\text{CO}_2$  (5 mbar) and  $\text{H}_2\text{O}$  ( $\sim 20$  mbar) at BT: HY (blue curve), MgO (dark grey curve), and MgOHY (red curve); (c) sample of part (b) subsequently outgassed at  $250\text{ }^\circ\text{C}$  for 120 min: HY (blue curve), MgO (dark grey curve), and MgOHY (red curve).

The hydration of  $\text{CO}_2/\text{MgOHY}$  was monitored in time in order to better understand the effect of  $\text{H}_2\text{O}$  upon  $\text{CO}_2$  adsorption (see Figure 3). The IR spectrum obtained after contact with 5 mbar of  $\text{CO}_2$  (orange line) shows only the signal associated to  $\text{CO}_2\text{-Mg}^{2+}$  adducts (*vide supra*). When  $\text{H}_2\text{O}$  is admitted into the cell, a component of the  $\nu_3(\text{CO}_2)$  band grows at  $2343\text{ cm}^{-1}$  (yellow line), ascribed to  $\text{CO}_2\text{-(H}_2\text{O/Mg}^{2+})$ .<sup>32</sup> The evolution of the spectra in the following 15 min (illustrated by grey curves in Figure 3a) highlights, in the  $2400\text{-}2300\text{ cm}^{-1}$  region, a fast decrease in the intensity of all the spectral components. Meanwhile, in the region of the carbonates, we observe the growth of four main groups of bands, whose detailed assignment is biased by the presence of components in the background (see Figure S1) and by the intense contribution of the bending mode of water final spectrum, red line). Such time evolution suggests that  $\text{H}_2\text{O}$ , while slowly diffusing within the zeolite pores, interacts with the MgO nanoclusters and promotes the reactivity of  $\text{CO}_2$  with the adsorbent, as the decrease in the intensity of  $\nu_3$  and the simultaneous growth of the bands assigned to the  $\delta(\text{HOH})$  mode of water and to (bi)carbonates testify. Figure 3b illustrates the main desorption steps, showing that not only the remaining fraction of linearly adsorbed  $\text{CO}_2$  are reversible at RT, but also the majority of carbonates upon a prolonged outgassing in dynamic vacuum (12 h, brown curve). Finally, by increasing the temperature to  $250\text{ }^\circ\text{C}$  for 60 min, a

spectrum is obtained (black curve) closely similar to the one of the starting material (*i.e.* activated *in vacuo* at 400 °C), suggesting a complete reversibility of all the species originated from CO<sub>2</sub>.

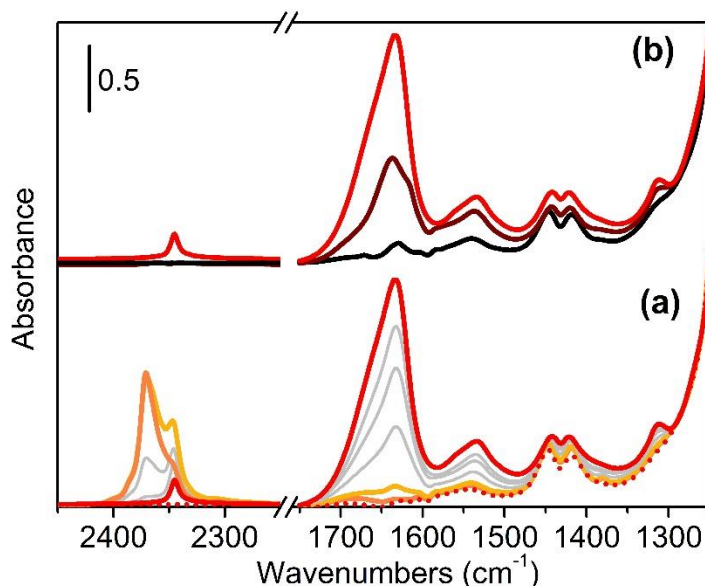


**Figure 3.** IR spectra in the regions relative to linear CO<sub>2</sub> complexes (2500-2200 cm<sup>-1</sup>) and to (bi)carbonate-like species (1800-1200 cm<sup>-1</sup>) of: **(a)** MgOHY after activation at 400 °C (dotted red curve, see Figure S1), upon contact with 5 mbar of pure CO<sub>2</sub> (orange curve), upon dosage of H<sub>2</sub>O vapor pressure on the pre-adsorbed CO<sub>2</sub> (yellow curve) and after a contact of 15 min with the CO<sub>2</sub>/H<sub>2</sub>O mixture (red curve); light grey spectra report the time evolution as observed *in situ* after the dosage of H<sub>2</sub>O; and **(b)** MgOHY after 15 min contact with the CO<sub>2</sub>/H<sub>2</sub>O mixture (red curve), thus outgassed at RT for 12 h (brown curve) and at 250 °C for 1 h (black curve).

The experiments described above have shown that, in spite of the hydrophilicity of the zeolite, CO<sub>2</sub> can still adsorb in presence of H<sub>2</sub>O on MgOHY, eventually involving some synergic effects between the two adsorbates and bringing to the chemical fixation of CO<sub>2</sub>. This is in agreement

with previous reports on bulk oxides.<sup>8</sup> Moreover, the nanoconfinement of MgO by the zeolite pores significantly decreases the regeneration of the material with respect to that typical of MgO.

MgOHY has been then investigated by an *in situ* IR-MS experiment, mimicking a post-combustion process (see Figure 4). The experiment was conducted in flow where the sample was (i) activated in dry He, (ii) exposed to a mixture simulating a post combustion exhaust for 15 h at 25 °C, and (iii) regenerated in a dry He flow at increasing temperature (see the Experimental section for details). The spectrum obtained after activation in He is characterized by a nearly flat profile in the  $1400 < \nu < 3000 \text{ cm}^{-1}$  region, testifying a more effective activation of the sample in these conditions with respect to vacuum (dotted red line in part a of Figure 4). The time evolution of the spectra is illustrated by the grey lines in Figure 4a, until the final state is reached, reported as a red curve. By comparing the spectra profiles obtained in static (Figure 3a) and dynamic (Figure 4a) conditions, it is evident that in the latter case CO<sub>2</sub> competes more efficiently in being adsorbed in the composite, with respect to what has been observed in static conditions. The nature of the formed species is identical, although changed in their relative abundance. The effective sequestration of CO<sub>2</sub> is confirmed by MS data presented in panels (I) and (II) of Figure 4, that show the signals of H<sub>2</sub>O ( $m/z = 18$ ) and CO<sub>2</sub> ( $m/z = 44$ ) in the flow downstream the IR cell, respectively. In fact, the H<sub>2</sub>O signal gradually increases since early experiment stages, reaching a plateau after ~300 min. On the other hand, the CO<sub>2</sub> signal remains constantly low at its initial value over the same time period, then abruptly increases as adsorption capacity of MgOHY toward the CO<sub>2</sub>/H<sub>2</sub>O mixture is reached. The bands of molecularly adsorbed CO<sub>2</sub> during the experiment (reported in the Supporting Information as Figure S3) show that besides the chemisorption with formation of carbonates, adsorption of molecular CO<sub>2</sub> is also significant in MgOHY. It is noteworthy that during this flow experiment, vibrations of molecularly adsorbed CO<sub>2</sub> are observed

both at  $2370\text{ cm}^{-1}$  (linear coordination to  $\text{Mg}^{2+}$  sites) and at lower frequencies, peaked and  $2343$  and  $2354\text{ cm}^{-1}$  (physisorbed and weakly interacting). This is in contrast with what observed in static experiments, where only a weak band of physisorbed/weakly interacting  $\text{CO}_2$  was left after water dosage. This finding indicates that  $\text{H}_2\text{O}$  adsorption does not block the  $\text{CO}_2$  adsorption mechanism in the realistic post-combustion conditions adopted in the flow experiment.

The spectra recorded during the sample regeneration are reported in Figure 4b. The red line refers to the equilibrated spectrum collected after 15 h of exposure to the  $\text{CO}_2/\text{H}_2\text{O}$  flow. Orange spectra have been collected in pure He flow, starting from RT and rising progressively the temperature till  $200\text{ }^\circ\text{C}$ . As it is clearly seen, the desorption of carbonates is nearly complete at the end of the process, as all their absorption bands (doublet at  $1310\text{ cm}^{-1}$  and  $1670\text{ cm}^{-1}$ , broad bands in the  $1350\text{-}1600\text{ cm}^{-1}$  range) are nicely eroded. Thermal treatments at higher temperature, from  $200\text{ }^\circ\text{C}$  to  $450\text{ }^\circ\text{C}$  (spectra in light orange), affect mostly the band at  $1633\text{ cm}^{-1}$ , due to the  $\delta(\text{HOH})$  mode of residual adsorbed water, and the already weak carbonates bands. When the sample reaches  $500\text{ }^\circ\text{C}$  in pure He flux, (red dotted curve in Figure 4b), the spectrum of the pristine activated material is restored. Panels (III) and (IV) of Figure 4 show the MS signals of  $\text{H}_2\text{O}$  and  $\text{CO}_2$  during desorption. Water is desorbed in two steps: a first release occurs at RT; a second one is observed upon heating, with a peak at about  $150^\circ\text{C}$  and being complete around  $300^\circ\text{C}$ .  $\text{CO}_2$  is released in three steps: the majority of it is released at RT. A second release occurs simultaneously with the release of water peaked at  $150^\circ\text{C}$ , while a last, small fraction is released only between  $400$  and  $500^\circ\text{C}$ .

These results confirm the high affinity of the material for  $\text{CO}_2$ , even in presence of water, and associate it to the nanoconfined  $\text{MgO}(\text{H})$  species. The efficient capture of  $\text{CO}_2$  in the initial part of the adsorption experiment demonstrate that  $\text{CO}_2$  and water can both favorably adsorb on the

material. Upon desorption, the carbonates are desorbed simultaneously with water in two steps at low temperature ( $< 200\text{ }^{\circ}\text{C}$ ), with only a residual fraction desorbed in “almost dry” conditions above  $400^{\circ}\text{C}$ . These results are very interesting both from a practical and fundamental point of view: on one hand, they demonstrate the feasibility of reversible  $\text{CO}_2$  adsorption from a wet stream, a subject which will be more deeply (and quantitatively) investigated in a future publication. On the other hand, they confirm the importance of water in enhancing the adsorption process, furthermore promoting the formation of species characterized by a low decomposition temperature.

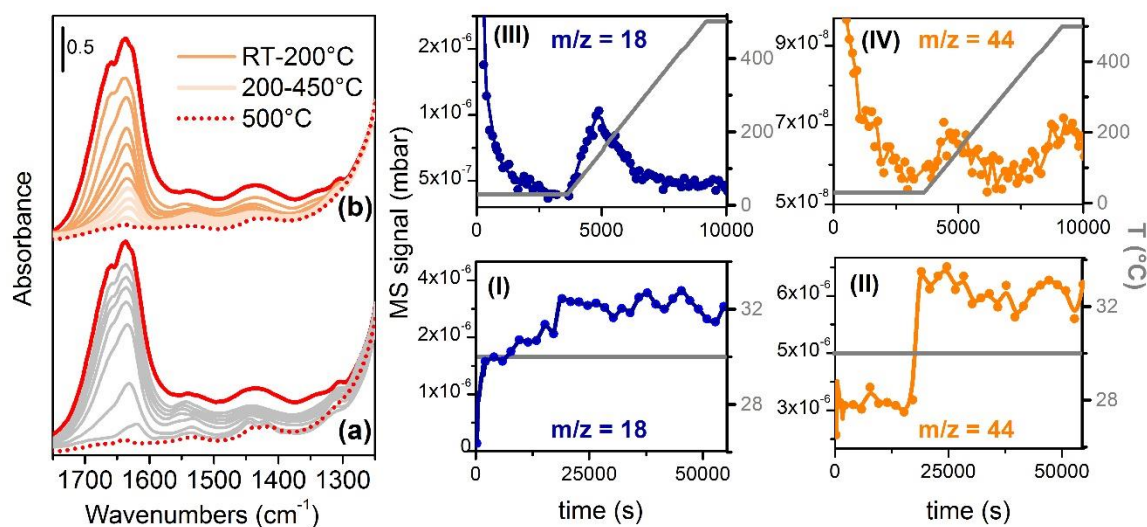


**Figure 4.** *In situ* IR spectra in the spectral regions relative to carbonate-like species ( $1800\text{--}1200\text{ cm}^{-1}$ ) of MgOHY. (a) Adsorption run. MgOHY after activation at  $400^{\circ}\text{C}$  (dotted red curve) and upon contact for 15 h with a  $\text{CO}_2/\text{H}_2\text{O}$  flow at  $30^{\circ}\text{C}$  (red solid curve). Light grey lines: spectra recorded in time. (b) Desorption run. MgOHY after 15 h of contact with a  $\text{CO}_2/\text{H}_2\text{O}$  flow at  $30^{\circ}\text{C}$  (red curve) and after desorption in a dry He flow at RT- $200^{\circ}\text{C}$  (orange curves),  $200\text{--}450^{\circ}\text{C}$  (light orange curves) and  $500^{\circ}\text{C}$  (red dotted curve). Right side of the figure shows the MS signals of  $\text{H}_2\text{O}$  (dark blue,  $m/z=18$  amu) and  $\text{CO}_2$  (orange,  $m/z=44$  amu) proper of the flow downstream the

IR cell, collected during the adsorption (panels (I) and (II)) and the desorption runs (panels (III) and (IV)) of the experiment.

*Periodic DFT calculations.* H<sub>2</sub>O/CO<sub>2</sub> adsorption properties of MgOHY have been investigated by means of state of the art periodic quantum mechanical methods. In particular, we aimed at explaining the observed low temperature reversibility and the H<sub>2</sub>O/CO<sub>2</sub> interplay.

Models for MgOHY are taken from a previous study of the material.<sup>16</sup> In that work, two types of structural motifs have been proposed for the MgO(H) species hosted in the HY framework: (i) (MgO)<sub>4</sub> cubelets representative of the structures where the short-range order of the MgO bulk structure is partially retained (*cube1* and *cube2* in the following), and (ii) “brucite like” open structures, where (MgO)<sub>n</sub> moieties interact more strongly with the zeolite pore walls (*brucite-like model*). These models were obtained by simulated reaction of (MgO)<sub>4</sub> units with the protons of zeolite Y and therefore contain a variable number of OH groups. These two typologies of models are not intended as the exact structures of all the MgO species, but only as suggested typologies mimicking the properties of the real material. Indeed, based on the results on a large set of candidate structures examined in the previous work,<sup>16</sup> we assume that a variety of sites with broad variability of Mg nuclearity may occur in the MgOHY material, whose local structure however resembles one of the above mentioned models.<sup>16</sup>

In the context of the present work, these results needed to be framed within a better understanding of the CO<sub>2</sub> interaction in presence of multiple H<sub>2</sub>O molecules. For this reason, the hydration of the models with up to three water molecules has been studied first. The hydrated models have been constructed by manually placing the water molecule close to the 3-, 4-, and 5-coordinated Mg

atoms. We report and comment here the results obtained for the hydration of initially 3-coordinated sites. Some representative structures are presented in Figure 6, and all the structures are reported numerically in the Supporting Information. The H<sub>2</sub>O adsorption energies, enthalpies and Gibbs free energies are reported in Table 2.

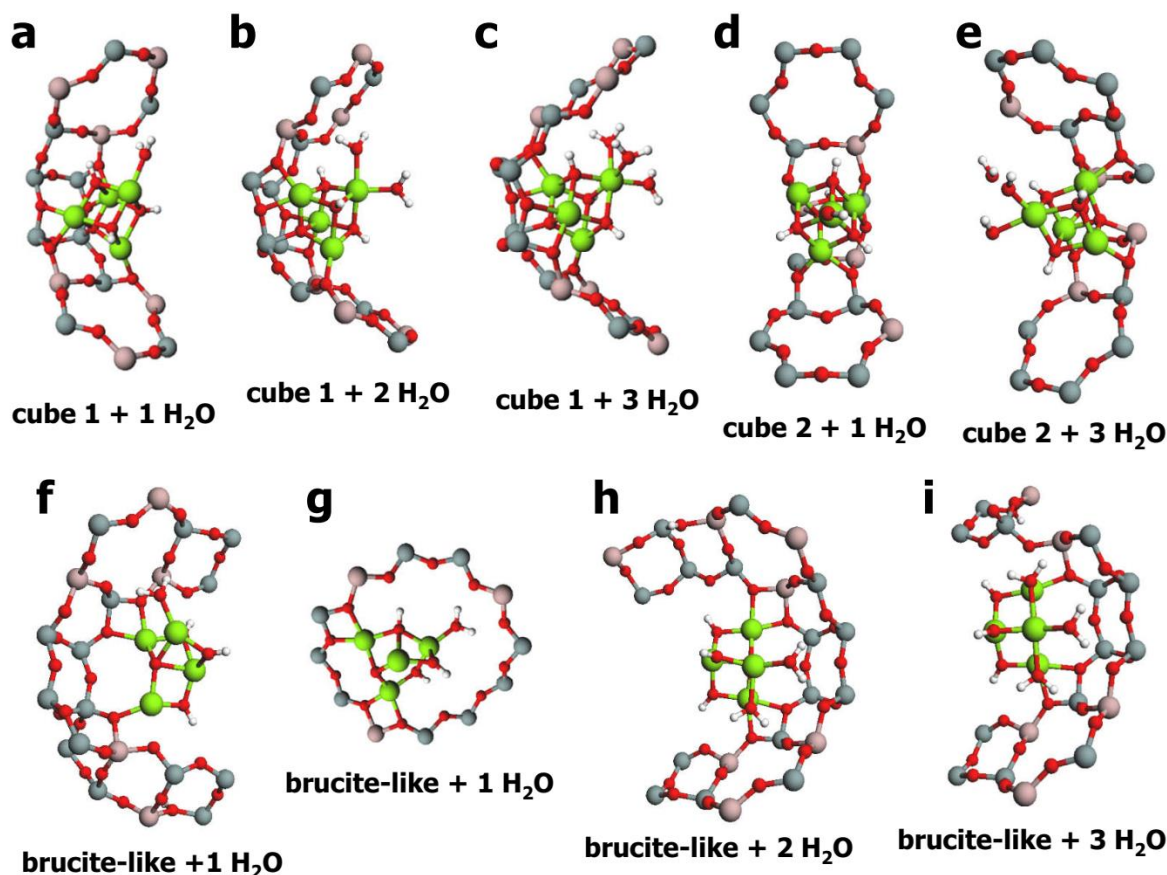


**Figure 6.** Structures of water adducts with representative (MgO)<sub>4</sub> structures in MgOHY (*cube 1*, *cube 2*, and *brucite-like*) as obtained by optimization at the B3LYP-D\* level (color code: Si = grey, Al = pink, O = red, H = white, and Mg = green).

**Table 2.** Computed binding energies  $\Delta E$ , enthalpies  $\Delta H$  and free energies  $\Delta G$  for the adsorption of  $\text{H}_2\text{O}$  onto 3-coordinated  $\text{Mg}^{2+}$  sites of  $(\text{MgO})_4$  clusters hosted in MgOHY pores, by precoordinating  $n$   $\text{H}_2\text{O}$  molecules ( $n = 1, 2, 3$ ). Values as obtained by optimization at the B3LYP-D\* level.  $\Delta H$  and  $\Delta G$  have been evaluated at 1 atm and 25 °C.

<b>Model</b>	<b><math>\Delta E</math></b>	<b><math>\Delta H</math></b>	<b><math>\Delta G</math></b>
	<b>(kJ/mol)</b>	<b>(kJ/mol)</b>	<b>(kJ/mol)</b>
<i>cube 1 + 1H<sub>2</sub>O</i>	-198.8	-196.0	-150.7
<i>cube 1 + 2H<sub>2</sub>O</i>	-126.4	-118.8	-81.9
<i>cube 1 + 3H<sub>2</sub>O</i>	-95.0	-86.7	-43.7
<i>cube 2 + 1H<sub>2</sub>O</i> <sup>a</sup>	-231.7	-227.4	-188.3
<i>cube 2 + 2H<sub>2</sub>O</i>	-81.2	-74.5	-34.3
<i>cube 2 + 3H<sub>2</sub>O</i> <sup>b</sup>	-72.2	-62.6	-16.6
<i>open cube + 1H<sub>2</sub>O</i>	-293.9	-280.3	-226.7
<i>open cube + 2H<sub>2</sub>O</i>	-96.7	-88.6	-51.4
<i>open cube + 3H<sub>2</sub>O</i> <sup>b</sup>	-69.2	-69.0	-26.0
<i>brucite-like + 1H<sub>2</sub>O</i> <sup>c</sup>	-231.1	-223.1	-176.4
<i>brucite-like + 2H<sub>2</sub>O</i>	-205.5	-197.4	-149.4
<i>brucite-like + 3H<sub>2</sub>O</i>	-138.2	-129.3	-83.2

<sup>a</sup> dissociative adsorption, producing a basic Mg-OH termination; <sup>b</sup> one  $\text{H}_2\text{O}$  molecule interacts only through H-bond. <sup>c</sup> Structure f in Figure 6.

The adsorption of water is exothermic and thermodynamically favored for all the models considered. Non-dissociative adsorption is observed except for the first hydration of *cube 2* and one of the *brucite-like* models (see Figure 6d and 6f, respectively). This is not surprising considering that the  $(\text{MgO})_4$  clusters are already hydroxylated. All models are capable of binding



up to three water molecules with moderate to high strength (see Table 2).  $\Delta E$  magnitude decreases fast with the coverage, being significantly reduced already for the second water molecule. In a few cases (e.g. *cube 2* + 3  $H_2O$ , Figure 6e), the third water molecule is not coordinated to a magnesium atom, but it interacts through hydrogen bond with pre-adsorbed water molecules and with the zeolite framework. Water adsorption does not alter significantly the structure of *cube 1* and *cube 2*, as shown for example in structures a-e of Figure 6. The *brucite-like* cluster, conversely, experiences an extensive rearrangement upon hydration, as shown in models of Figure 6f-i. Moreover, the *brucite-like* cluster moves from the supercage to the 12-ring window connecting two supercages as clearly shown in Figure 6g. This location allows to maximize contact of the cluster with the zeolite wall through H-bonds with zeolite bridging oxygens.

Adsorption of  $CO_2$  has been modeled for dehydrated MgOHY structures and for some of the  $(H_2O)_n$ -MgOHY models presented above. In these simulations, the final optimized geometry strongly depends on the starting geometry of the models, testifying the presence of a complex potential energy surface with several minima. In order to sample this complex surface, starting geometries were constructed in three different ways. (i)  $CO_2$  was coordinated through the oxygen atom to the least-coordinated Mg atom of the clusters: the optimization of these models led in most cases to linear complexes. (ii)  $CO_2$  was coordinated via the carbon atom to the least coordinated oxygen atom of the cluster: the optimized structures were coincident with those obtained in (i). (iii) The carbon atom of  $CO_2$  was placed at a very short contact from one low-coordination basic oxygen of the clusters: the optimized structures resulted in the formation of carbonate and bicarbonate species.

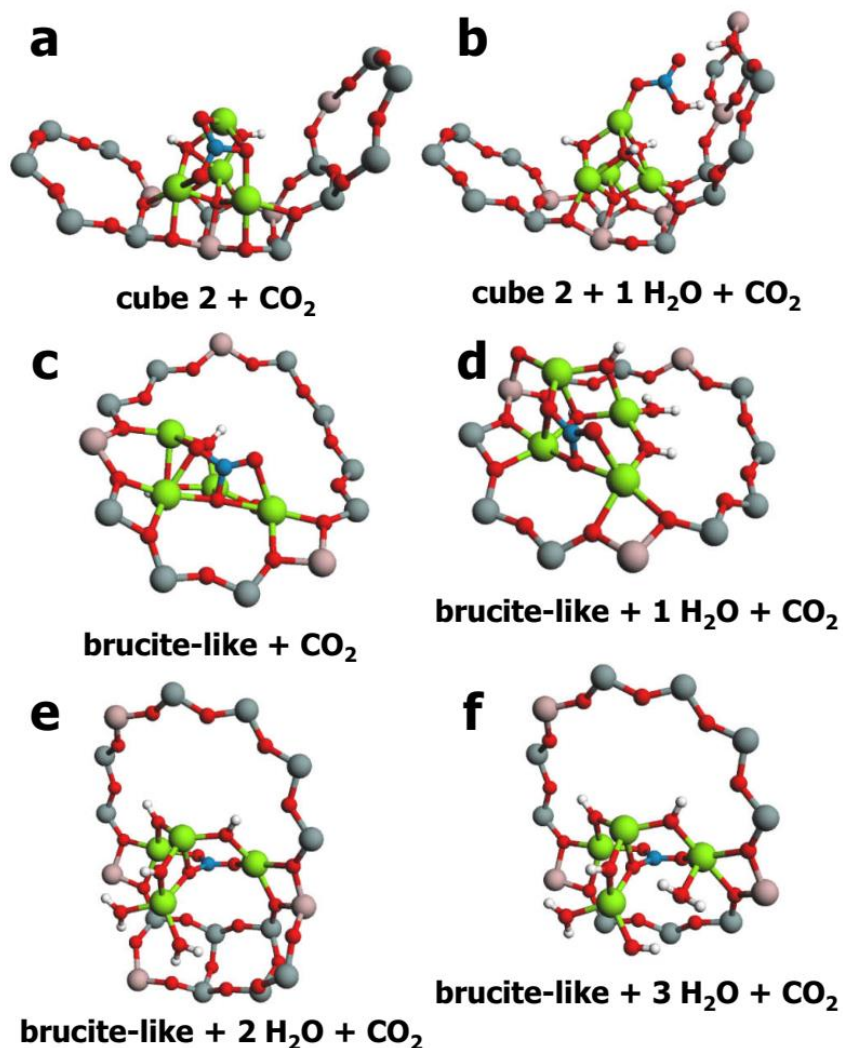


**Figure 7.** Structures optimized at the B3LYP-D\* level of carbonates and bicarbonates obtained by CO<sub>2</sub> reaction with the (MgO)<sub>4</sub> models *cube 1*, *cube 2*, and *brucite-like* for different degrees of hydration. Color codes: Si = grey, Al = pink, O = red, Mg = green, C = blue, H = white.

**Table 3.** Formation energies  $\Delta E$ , enthalpies  $\Delta H$  and free energies  $\Delta G$  for selected CO<sub>2</sub> adducts with (MgO)<sub>4</sub> clusters in MgOHY (*ion-exchange site*, *cube 1*, *cube 2*, *open cube*, and *brucite-like*)

as obtained at the B3LYP level by considering different degrees of hydration.  $\Delta H$  and  $\Delta G$  have been evaluated at 1 atm and 25 °C.

Model	Type of adduct	$\Delta E$ (kJ/mol)	$\Delta H$ (kJ/mol)	$\Delta G$ (kJ/mol)
<i>ion-exchange site</i> + $CO_2$ <sup>a</sup>	linear	-65.8	-61.1	-20.5
<i>cube 1</i> + $CO_2$ <sup>a</sup>	linear	-104.2	-103.8	-68.2
<i>cube 2</i> + $CO_2$ <sup>a</sup>	linear	-66.2	-64.7	-21.1
<i>open cube</i> + $CO_2$ <sup>a</sup>	bicarbonate	-18.6	-11.4	37.7
<i>brucite-like</i> + $CO_2$ <sup>a</sup>	linear	-113.7	-110.1	-71.8
<i>cube 2</i> + $CO_2$ (a) <sup>b</sup>	carbonate	-221.0	-215.0	-165.4
<i>cube 2</i> + 1 $H_2O$ + $CO_2$ (b) <sup>b</sup>	bicarbonate	-90.9	-87.1	-31.9
<i>brucite-like</i> + $CO_2$ (c) <sup>b</sup>	carbonate	-343.0	-338.0	-284.4
<i>brucite-like</i> + 1 $H_2O$ + $CO_2$ (d) <sup>b</sup>	carbonate	-193.9	-189.4	-140.0
<i>brucite-like</i> + 2 $H_2O$ + $CO_2$ (e) <sup>b</sup>	carbonate	-179.8	-175.5	-128.7
<i>brucite-like</i> + 3 $H_2O$ + $CO_2$ (f) <sup>b</sup>	carbonate	-165.3	-160.8	-112.7

<sup>a</sup> data from ref <sup>16</sup>; <sup>b</sup> numeric labels in brackets refer to models reported in Figure 7.

The linear complexes obtained by optimizing starting geometries of (i) and (ii) kind are characterized by formation enthalpies ranging from -61.1 to -103.8 kJ/mol (see Table 3 and ref. <sup>16</sup>). A low formation enthalpy bicarbonate (-11.4 kJ/mol) is predicted only in the case of the *open cube* model.<sup>16</sup> These binding energies are on average lower than those observed for  $H_2O$  molecules (see Table 2).

The structures obtained using the (iii) strategy are reported in Figure 7 and their formation energies are listed in Table 3. In this case, the energies are comparable with those observed for  $H_2O$  molecules on the same models (see Table 2). Model *cube 2* forms a tridentate carbonate with a

reaction enthalpy of -215.0 kJ/mol (Figure 7a), while the more flexible *brucite-like* model forms a carbonate with a remarkable reaction enthalpy of -338.0 kJ/mol (Figure 7, model). The value obtained for *cube 2* is close to that reported for the formation of the same species on corners present on the surface of bulk MgO.<sup>41</sup> The formation of carbonates on models coordinating one H<sub>2</sub>O molecule was also explored for *cube 2* and *brucite-like* models. In both cases, the presence of water makes the process less exothermic by more than 100 kJ mol<sup>-1</sup>. On cubic models (*cube 2* + 1 H<sub>2</sub>O, Figure 6d), the presence of water also causes a change in the formed species, a bicarbonate instead of a carbonate (Figure 7b). These results indicate that the presence of moisture, while not affecting the adsorption properties of MgOHY (being the reaction enthalpies very high, < -90 kJ mol<sup>-1</sup>), allows forming chemisorbed species characterized by a lower stability than those that would be formed in dry conditions, that would then require a lower regeneration energy. This finding supports in a quantitative manner the experimental results reported in the MgO literature.<sup>8</sup> The dependence of the carbonate formation enthalpy on the hydration degree was also studied for the *brucite-like* model, considering the presence of 1, 2, and 3 water molecules (Figure 7d-f). The exothermicity of the process only slightly decreases upon addition of the second and the third water molecule (from -189.4 to -175.5 and -140.8 kJ/mol, respectively), indicating that water concentration higher than that the stoichiometric amount are to be preferred, although a too large water concentration is not expected to bring a significant benefit.

## Conclusions

The spectroscopic and computational results discussed above contribute to explain the affinity of MgOHY for CO<sub>2</sub> in wet streams and the reversibility of its adsorption. Spectroscopic data suggested a synergetic interplay of CO<sub>2</sub> and H<sub>2</sub>O, the latter seeming to facilitate the formation reaction of carbonate and bicarbonate-like species responsible for the carbon dioxide uptake of the

material in wet conditions. The same observation stands in both model (static atmosphere) and realistic (flow) reaction environments. Modelling consistently predicts the formation of stable carbonate and bicarbonate-like species by reaction of CO<sub>2</sub> with hydrated MgO nanoclusters. Interestingly, the binding energies of CO<sub>2</sub> and H<sub>2</sub>O are variable according to the site, but they constantly fall in the same energetic range, suggesting these molecules can effectively compete in the formation of stable adducts. Among the models investigated, the less-coordinated *brucite-like* display a stronger reactivity, as compared to the *cube 1* and *cube 2* models. The former have a remarkably flexible structure, which allows the interaction with several adsorbate molecules and the zeolite pore walls at the same time. In particular, water and bicarbonates are able to form strong hydrogen bonds bridging between MgO clusters and the zeolite pore walls. This coordination flexibility, made possible by the synergy between the small cluster size and the presence of the polar zeolite walls explains the reversibility of CO<sub>2</sub> adsorption and the low temperature of desorption, observed experimentally. In fact, stable carbonates are formed on active sites of the MgO clusters, but their small size avoids the formation of Madelung-stabilized bulk carbonates, whose stability would be associated to a high decomposition temperature. Generalizing, these results show that highly dispersed MgO nanoclusters in a porous polar system enhancing their activity and protecting them from aggregation represent a promising direction for the development of robust and efficient CO<sub>2</sub> capture materials in presence of water.

### Supporting Information

IR spectra of the activated materials; Detail of the CO<sub>2</sub> molecular adducts region for the static IR experiments (complement to Figure 2); Detail of the CO<sub>2</sub> molecular adducts region for the in situ IR experiment (complement to Figure 4); basis sets adopted for calculations (MgOY\_CO2\_SI.pdf).

Selected optimized structures in .cif format (structures.zip).

This material is available free of charge via the Internet at <http://pubs.acs.org>.

### **Corresponding Author**

\* J. G. Vitillo, Department of Science and High Technology and INSTM, Università degli Studi dell'Insubria, Via Valleggio 9, I-22100 Como, Italy. Email: [jg.vitillo@gmail.com](mailto:jg.vitillo@gmail.com)

and

\* G. Ricchiardi, Università di Torino, Dipartimento di Chimica and NIS Interdepartment Centre, Via Giuria 7, 10125 Torino (Italy) Email: [gabriele.ricchiardi@unito.it](mailto:gabriele.ricchiardi@unito.it)

### **Author Contributions**

The manuscript was written through contributions of all authors. All authors have given approval to the final version of the manuscript.

### **Acknowledgments**

The simulations were performed on resources provided by UNINETT Sigma2 - the National Infrastructure for High Performance Computing and Data Storage in Norway, under project number NN9381K. Filippo Giordanino is acknowledged for the help in the infrared experiments.

## References

- (1) Vitillo, J. G.; Smit, B.; Gagliardi, L. Introduction: Carbon Capture and Separation. *Chem. Rev.* **2017**, *117* (14), 9521–9523. <https://doi.org/10.1021/acs.chemrev.7b00403>.
- (2) Rochelle, G. T. Amine Scrubbing for CO<sub>2</sub> Capture. *Science* (80-. ). **2009**, *325* (5948), 1652–1654. <https://doi.org/10.1126/science.1176731>.
- (3) Wang, J.; Huang, L.; Yang, R.; Zhang, Z.; Wu, J.; Gao, Y.; Wang, Q.; O'Hare, D.; Zhong, Z. Recent Advances in Solid Sorbents for CO<sub>2</sub> Capture and New Development Trends. *Energy Environ. Sci.* **2014**, *7* (11), 3478–3518. <https://doi.org/10.1039/C4EE01647E>.
- (4) Patel, H. A.; Byun, J.; Yavuz, C. T. Carbon Dioxide Capture Adsorbents: Chemistry and Methods. *ChemSusChem* **2017**, *10* (7), 1303–1317. <https://doi.org/10.1002/cssc.201601545>.
- (5) Wang, S.; Yan, S.; Ma, X.; Gong, J. Recent Advances in Capture of Carbon Dioxide Using Alkali-Metal-Based Oxides. *Energy Environ. Sci.* **2011**, *4* (10), 3805. <https://doi.org/10.1039/c1ee01116b>.
- (6) BARTHOMEUF\*, D. Basic Zeolites: Characterization and Uses in Adsorption and Catalysis. *Catal. Rev.* **1996**, *38* (4), 521–612. <https://doi.org/10.1080/01614949608006465>.
- (7) Maitra, A. M.; Campbell, I.; Tyler, R. J. Influence of Basicity on the Catalytic Activity for Oxidative Coupling of Methane. *Appl. Catal. A Gen.* **1992**, *85* (1), 27–46. [https://doi.org/10.1016/0926-860X\(92\)80127-X](https://doi.org/10.1016/0926-860X(92)80127-X).
- (8) Vitillo, J. G. Magnesium-Based Systems for Carbon Dioxide Capture, Storage and Recycling: From Leaves to Synthetic Nanostructured Materials. *Rsc Adv.* **2015**, *5* (46),

- 36192–36239. <https://doi.org/10.1039/c5ra02835c>.
- (9) Masala, A.; Vitillo, J. G.; Mondino, G.; Martra, G.; Blom, R.; Grande, C. A.; Bordiga, S. Conductive ZSM-5-Based Adsorbent for CO<sub>2</sub> Capture: Active Phase vs Monolith. *Ind. Eng. Chem. Res.* **2017**, *56* (30), 8485–8498. <https://doi.org/10.1021/acs.iecr.7b01058>.
  - (10) Bae, T.-H.; Hudson, M. R.; Mason, J. A.; Queen, W. L.; Dutton, J. J.; Sumida, K.; Micklash, K. J.; Kaye, S. S.; Brown, C. M.; Long, J. R. Evaluation of Cation-Exchanged Zeolite Adsorbents for Post-Combustion Carbon Dioxide Capture †. <https://doi.org/10.1039/c2ee23337a>.
  - (11) Su, F.; Lu, C. CO<sub>2</sub> Capture from Gas Stream by Zeolite 13X Using a Dual-Column Temperature/Vacuum Swing Adsorption. *Energy Environ. Sci.* **2012**, *5* (10), 9021. <https://doi.org/10.1039/c2ee22647b>.
  - (12) Li, G.; Xiao, P.; Webley, P.; Zhang, J.; Singh, R.; Marshall, M. Capture of CO<sub>2</sub> from High Humidity Flue Gas by Vacuum Swing Adsorption with Zeolite 13X. *Adsorption* **2008**, *14* (2–3), 415–422. <https://doi.org/10.1007/s10450-007-9100-y>.
  - (13) Shen, C. M.; Worek, W. M. Cosorption Characteristics of Solid Adsorbents. *Int. J. Heat Mass Transf.* **1994**, *37* (14), 2123–2129. [https://doi.org/10.1016/0017-9310\(94\)90313-1](https://doi.org/10.1016/0017-9310(94)90313-1).
  - (14) Bezerra, D. P.; Oliveira, R. S.; Vieira, R. S.; Cavalcante, C. L.; Azevedo, D. C. S. Adsorption of CO<sub>2</sub> on Nitrogen-Enriched Activated Carbon and Zeolite 13X. *Adsorption* **2011**, *17* (1), 235–246. <https://doi.org/10.1007/s10450-011-9320-z>.
  - (15) McDonald, T. M.; Mason, J. A.; Kong, X.; Bloch, E. D.; Gygi, D.; Dani, A.; Crocellà, V.;



- Giordanino, F.; Odoh, S. O.; Drisdell, W. S.; et al. Cooperative Insertion of CO<sub>2</sub> in Diamine-Appended Metal-Organic Frameworks. *Nature* **2015**, *519* (7543), 303–308. <https://doi.org/10.1038/nature14327>.
- (16) Vitillo, J. G.; Fjermestad, T.; D'Amore, M.; Milanesio, M.; Palin, L.; Ricchiardi, G.; Bordiga, S. On the Structure of Superbasic (MgO)<sub>n</sub> Sites Solvated in a Faujasite Zeolite. *Phys. Chem. Chem. Phys.* **2018**, *20* (27), 18503–18514. <https://doi.org/10.1039/C8CP01788C>.
- (17) Knözinger, E.; Jacob, K. H.; Singh, S.; Hofmann, P. Hydroxyl Groups as IR Active Surface Probes on MgO Crystallites. *Surf. Sci.* **1993**, *290* (3), 388–402. [https://doi.org/10.1016/0039-6028\(93\)90721-U](https://doi.org/10.1016/0039-6028(93)90721-U).
- (18) Erba, A.; Baima, J.; Bush, I.; Orlando, R.; Dovesi, R. Large-Scale Condensed Matter DFT Simulations: Performance and Capabilities of the CRYSTAL Code. *J. Chem. Theory Comput.* **2017**, *13* (10), 5019–5027. <https://doi.org/10.1021/acs.jctc.7b00687>.
- (19) Becke, A. D. A Multicenter Numerical Integration Scheme for Polyatomic Molecules. *J. Chem. Phys.* **1988**, *88* (4), 2547–2553. <https://doi.org/10.1063/1.454033>.
- (20) Yang, W.; Parr, R. G.; Lee, C. Various Functionals for the Kinetic Energy Density of an Atom or Molecule. *Phys. Rev. A* **1986**, *34* (6), 4586–4590. <https://doi.org/10.1103/PhysRevA.34.4586>.
- (21) Signorile, M.; Damin, A.; Bonino, F.; Crocellà, V.; Lamberti, C.; Bordiga, S. The Role of Dispersive Forces Determining the Energetics of Adsorption in Ti Zeolites. *J. Comput. Chem.* **2016**, *37* (30), 2659–2666. <https://doi.org/10.1002/jcc.24509>.

- (22) Signorile, M.; Damin, A.; Bonino, F.; Crocellà, V.; Ricchiardi, G.; Lamberti, C.; Bordiga, S. Computational Assessment of Relative Sites Stabilities and Site-Specific Adsorptive Properties of Titanium Silicalite-1. *J. Phys. Chem. C* **2018**, *122* (3), 1612–1621. <https://doi.org/10.1021/acs.jpcc.7b10104>.
- (23) Fischer, M. Water Adsorption in SAPO-34: Elucidating the Role of Local Heterogeneities and Defects Using Dispersion-Corrected DFT Calculations. *Phys. Chem. Chem. Phys.* **2015**, *17* (38), 25260–25271. <https://doi.org/10.1039/C5CP04189A>.
- (24) Fischer, M. Interaction of Water with (Silico)Aluminophosphate Zeotypes: A Comparative Investigation Using Dispersion-Corrected DFT. *Phys. Chem. Chem. Phys.* **2016**, *18* (23), 15738–15750. <https://doi.org/10.1039/C6CP02289H>.
- (25) Grimme, S. Semiempirical GGA-Type Density Functional Constructed with a Long-Range Dispersion Correction. *J. Comput. Chem.* **2006**, *27* (15), 1787–1799. <https://doi.org/10.1002/jcc.20495>.
- (26) Civalleri, B.; Zicovich-Wilson, C. M.; Valenzano, L.; Ugliengo, P. B3LYP Augmented with an Empirical Dispersion Term (B3LYP-D\*) as Applied to Molecular Crystals. *CrystEngComm* **2008**, *10* (4), 405–410. <https://doi.org/10.1039/B715018K>.
- (27) Nada, R.; Nicholas, J. B.; McCarthy, M. I.; Hess, A. C. Basis Sets for Ab Initio Periodic Hartree-Fock Studies of Zeolite/Adsorbate Interactions: He, Ne, and Ar in Silica Sodalite. *Int. J. Quantum Chem.* **1996**, *60* (4), 809–820. [https://doi.org/10.1002/\(sici\)1097-461x\(1996\)60:4<809::aid-qua3>3.0.co;2-0](https://doi.org/10.1002/(sici)1097-461x(1996)60:4<809::aid-qua3>3.0.co;2-0).
- (28) Catti, M.; Valerio, G.; Dovesi, R.; Causà, M. Quantum-Mechanical Calculation of the Solid-

- State Equilibrium  $\text{MgO}+\text{-Al}_2\text{O}_3\text{MgAl}_2\text{O}_4$  (Spinel) versus Pressure. *Phys. Rev. B* **1994**, *49* (20), 14179–14187. <https://doi.org/10.1103/PhysRevB.49.14179>.
- (29) Schäfer, A.; Horn, H.; Ahlrichs, R. Fully Optimized Contracted Gaussian Basis Sets for Atoms Li to Kr. *J. Chem. Phys.* **1992**, *97* (4), 2571–2577. <https://doi.org/10.1063/1.463096>.
- (30) Ugliengo, P.; Damin, A. Are Dispersive Forces Relevant for CO Adsorption on the  $\text{MgO}(001)$  Surface? *Chem. Phys. Lett.* **2002**, *366* (5–6), 683–690. [https://doi.org/10.1016/s0009-2614\(02\)01657-3](https://doi.org/10.1016/s0009-2614(02)01657-3).
- (31) Dovesi, R.; Saunders, V. R.; Roetti, C.; Orlando, R.; Zicovich-Wilson, C. M.; Pascale, F.; Civalleri, B.; Doll, K.; Harrison, N. M.; Bush, I. J.; et al. CRYSTAL17 User's Manual <http://www.crystal.unito.it/Manuals/crystal17.pdf>.
- (32) Bonelli, B.; Onida, B.; Fubini, B.; Otero Areán, C.; Garrone, E. Vibrational and Thermodynamic Study of the Adsorption of Carbon Dioxide on the Zeolite Na - ZSM-5. *Langmuir* **2000**, *16* (11), 4976–4983. <https://doi.org/10.1021/la991363j>.
- (33) Vitillo, J. G.; Savonnet, M.; Ricchiardi, G.; Bordiga, S. Tailoring Metal-Organic Frameworks for  $\text{CO}_2$  Capture: The Amino Effect. *ChemSusChem* **2011**, *4* (9), 1281–1290. <https://doi.org/10.1002/cssc.201000458>.
- (34) Areán, C. O.; Delgado, M. R. Variable-Temperature FT-IR Studies on the Thermodynamics of Carbon Dioxide Adsorption on a Faujasite-Type H-Y Zeolite. *Appl. Surf. Sci.* **2010**, *256* (17), 5259–5262. <https://doi.org/10.1016/j.apsusc.2009.12.114>.
- (35) Ramis, G.; Busca, G.; Lorenzelli, V. Low-Temperature  $\text{CO}_2$  adsorption on Metal Oxides: Spectroscopic Characterization of Some Weakly Adsorbed Species. *Mater. Chem. Phys.*

- 1991**, 29 (1–4), 425–435. [https://doi.org/10.1016/0254-0584\(91\)90037-U](https://doi.org/10.1016/0254-0584(91)90037-U).
- (36) Llabrés i Xamena, F. X.; Zecchina, A. FTIR Spectroscopy of Carbon Dioxide Adsorbed on Sodium- and Magnesium-Exchanged ETS-10 Molecular Sieves. *Phys. Chem. Chem. Phys.* **2002**, 4 (10), 1978–1982. <https://doi.org/10.1039/b110483g>.
- (37) Valenzano, L.; Civalleri, B.; Chavan, S.; Palomino, G. T.; Areán, C. O.; Bordiga, S. Computational and Experimental Studies on the Adsorption of CO, N<sub>2</sub>, and CO<sub>2</sub> on Mg-MOF-74. *J. Phys. Chem. C* **2010**, 114 (25), 11185–11191. <https://doi.org/10.1021/jp102574f>.
- (38) Busca, G.; Lorenzelli, V. Infrared Spectroscopic Identification of Species Arising from Reactive Adsorption of Carbon Oxides on Metal Oxide Surfaces. *Mater. Chem.* **1982**, 7 (1), 89–126. [https://doi.org/10.1016/0390-6035\(82\)90059-1](https://doi.org/10.1016/0390-6035(82)90059-1).
- (39) Wei, Y. L.; Wang, Y. M.; Zhu, J. H.; Wu, Z. Y. In-Situ Coating of SBA-15 with MgO: Direct Synthesis of Mesoporous Solid Bases from Strong Acidic Systems. *Adv. Mater.* **2003**, 15 (22), 1943–1945. <https://doi.org/10.1002/adma.200305803>.
- (40) Zhang, L.; Pham, T. N.; Faria, J.; Santhanaraj, D.; Sooknoi, T.; Tan, Q. H.; Zhao, Z.; Resasco, D. E. Synthesis of C-4 and C-8 Chemicals from Ethanol on MgO-Incorporated Faujasite Catalysts with Balanced Confinement Effects and Basicity. *ChemSusChem* **2016**, 9 (7), 736–748. <https://doi.org/10.1002/cssc.201501518>.
- (41) Jensen, M. B.; Pettersson, L. G. M.; Swang, O.; Olsbye, U. CO<sub>2</sub> Sorption on MgO and CaO Surfaces: A Comparative Quantum Chemical Cluster Study. *J. Phys. Chem. B* **2005**, 109 (35), 16774–16781. <https://doi.org/10.1021/jp052037h>.



TOC FIGURE

